RESEARCH ARTICLE

Author Contributions:
**Conceptualization:** F. Marra, F. Florindo
Funding acquisition: F. Florindo
Investigation: F. Marra, F. Florindo, M. Gaeta, B. R. Jicha
Writing – original draft: F. Marra, F. Florindo
Writing – review & editing: F. Marra, F. Florindo, M. Gaeta, B. R. Jicha

$^{40}Ar/^{39}Ar$ Age Constraints on MIS 5.5 and MIS 5.3 Paleo-Sea Levels: Implications for Global Sea Levels and Ice-Volume Estimates

F. Marra[1] , **F. Florindo[1]** , **M. Gaeta[2]** , and **B. R. Jicha[3]**

[1]Istituto Nazionale di Geofisica e Vulcanologia, Rome, Italy, [2]Dipartimento di Scienze della Terra, "Sapienza" Università di Roma, Roma, Italy, [3]Department of Geoscience, University of Wisconsin-Madison, Madison, WI, USA

Abstract We integrate 10 new with five published $^{40}Ar/^{39}Ar$ age determinations, both on primary volcanic deposits and on detrital sanidine, which provide precise geochronologic control on the Marine Isotope Stage (MIS) 5.5 and MIS 5.3 sea-level indicators that occur at three coastal caves in a tectonically stable region of the central Tyrrhenian Sea of Italy. The age of a *Strombus*-bearing bioclastic conglomerate, associated with a tidal notch occurring at 9.5 m a.s.l. at Cape Circeo, is constrained to between 121.5 ± 5.8 and 116.2 ± 1.2 ka. Moreover, backbeach deposits intercalated in the sedimentary filling of Guattari and Capre coastal caves are directly correlated with a tidal notch at ~2.5 m associated with another bioclastic conglomerate at Cape Circeo and dated to 110.4 ± 1.4–104.9 ± 0.9 ka. The latter deposit is also correlated with the adjacent marine terrace, occurring at 3–5 m on the coast between Capes Circeo and Anzio, for which a maximum age of 100.7 ± 6.6 ka was previously reported. These data provide evidence for a maximum sea level around 9.5 m above the present sea level and a duration of MIS 5.5 highstand until 116 ka, in agreement with estimates from other regions in the world. In contrast, they suggest a maximum sea level during MIS 5.3 highstand that is similar to the present level, and only ~7 m lower than the MIS 5.5 highstand, challenging the reconstructions of the MIS 5 ice-sheet volumes and derived global sea levels that are based on benthic oxygen isotope records.

1. Introduction

In light of the great importance that the studies on the assessment of sea-level variations due to ice melting have assumed in consequence of the current global warming (e.g., Box et al., 2022), there is a renewed interest at present in understanding the timing and magnitude of past sea levels.

Recent research has suggested evidence for paleo-sea levels much higher than those predicted by models based on the $\delta^{18}O$ records during the Marine Isotope Stage (MIS) 5.3 (~100 ka) and MIS 5.1 (~80 ka) highstands in the Mediterranean Sea (Dorale et al., 2010; Marra, Bahain, et al., 2019; Marra, Florindo, et al., 2016; Marra, Rolfo, et al., 2020; Marra et al., 2023; Vicens et al., 2012). The mismatch has important implications for the study of paleoclimate, as well as for the assessment of future scenarios linked to anthropogenic global warming. However, a key approach to demonstrate such discrepancy relies on the exact dating of the paleo-sea-level indicators, which so far is substantially limited to the U/Th method applied to corals or speleothems. Both of these applications have their own limitations (see Pasquetti et al., 2021, for a review) and have provided contrasting results for MIS 5.3 and MIS 5.1 worldwide (e.g., Medina-Elizalde, 2012; Wehmiller et al., 2004). Most of the "anomalous" sea levels during these highstands are inferred to be the result of modeled Glacial Isostatic Adjustment (GIA) processes (e.g., Muhs et al., 2012). However, in several unexplained cases, unforeseen "tectonic" issues are invoked, as well as possible incorrect age assessment (e.g., Medina-Elizalde, 2012; Muhs et al., 2015).

An alternative dating method, $^{40}Ar/^{39}Ar$ dating of detrital sanidine, has been applied recently to beach, lagoon, and backbeach deposits associated with the MIS 5 sea-level indicators on the Tyrrhenian Sea coast of central Italy, providing promising results (Marra, Gaeta, et al., 2019; Marra, Pereira, et al., 2021; Marra et al., 2023).

Besides providing maximum ages to the deposits, this dating approach has been effective in several cases in providing actual depositional ages. Use of this dating technique exploits the intense, continuous volcanic activity that has occurred in central Italy over the entire Pleistocene (see Marra, Gaeta, et al., 2019; Marra, Pereira, et al., 2021, for an in-depth discussion). Thus, the time of deposition is constrained between the age of the youngest crystal(s population) within a deposit and the age of the next eruption that occurred after its deposition.

Considering a recurrence interval on the order of the thousands of years (Marra, Castellano, et al., 2020; Marra et al., 2004), the youngest crystal (population) age in a sample is inferred to be a close match to the time of sediment deposition.

This is a statistical approach, which has good probability of success only when a large number of crystals are dated. Furthermore, it is assumed that the crystals from the most recent eruptions are eroded, transported, and redeposited within the sediment of interest.

Moreover, further limitations to the application of this dating method derive from the timing, intensity, and recurrence of volcanic activity in the so-called Roman Province, including the volcanic districts of Latium and Campania (Peccerillo, 2017, and ref. therein). This method has application between 800 and 200 ka when there was abundant volcanic activity, but it is strongly hampered between 200 and 120 ka in Latium, where there was a drastic reduction, or even a cessation, of volcanic activity during this time span (Marra, Castellano, et al., 2020, and ref. therein). In contrast, intense volcanic activity resumed in the interval 120 ka–present in the Campanian districts of Phlegraean Fields and Ischia Island (Monaco et al., 2022; Poli et al., 1987; Wulf et al., 2012), which are closer to the coastal sector investigated in the present study (Figure 1). Hence, there is the potential to precisely date sea-level changes during the 125 ka–present time frame.

With all of these factors in mind, in this paper, we provide indirect $^{40}Ar/^{39}Ar$ age constraints on the MIS 5.5 and 5.3 local sea-level highstands, both through dating of detrital sanidine and primary volcanic deposits. We do so by correlation of the sedimentary records of Guattari Cave (GC), Capre Cave (CC), and Moscerini Cave (MC), located along the coast of Latium (Tyrrhenian Sea, central Mediterranean; Figure 1), with the sea-level indicators reported in the literature, including the previously $^{40}Ar/^{39}Ar$ dated MIS 5.3 marine terrace (Borgo Hermada morpho-pedo-stratigraphic complex; Marra et al., 2023; Sevink et al., 1982) along the coast between Cape Circeo and Cape Anzio.

The 10 new $^{40}Ar/^{39}Ar$ ages reported here have been determined from primary pumice fragments and one primary tephra layer collected in the sedimentary infill of MC and CC, as well as from reworked sanidine crystals extracted from the sedimentary fill of CC and GC. We integrate these geochronological data with a previous set of five $^{40}Ar/^{39}Ar$ ages on detrital sanidine recently reported from the sedimentary deposits of GC and of the marine terrace deposits on the Pontine Plain (Marra et al., 2023).

2. Methods

2.1. $^{40}Ar/^{39}Ar$ Analysis

Ten $^{40}Ar/^{39}Ar$ age determinations were performed on sanidine crystals extracted from either samples of primary or reworked volcanic deposits, as well as from sedimentary deposits.

Samples dated for the present work are as follows:

- Two pumice clasts (MOSC-22, MOSC-37) extracted from the sand layers constituting the sedimentary fill of MC, recovered during the original archeological excavations performed in the year 1949, stored at the Istituto Italiano di Paleontologia Umana (IIPU) repository in Anagni (Frosinone, Italy).
- One tephra layer (sample GDC-10) intercalated in the sedimentary fill of CC.
- Seven sedimentary sand samples collected at CC (GDC-6, GDC-8, and GDC-0) and GC (GU-1, GU-5, GU-105, and GU-116). These latter samples integrate five age determinations on reworked sanidine crystals previously performed at GC (Marra et al., 2023).

Sanidine phenocrysts were ultrasonically leached in 3 M HCl for 10 min, rinsed repeatedly with deionized water, and then ultrasonically leached in 1.5 M HF for several minutes, followed by additional rinses in deionized water. Sanidine phenocrysts were coirradiated with the 1.1864 Ma Alder Creek sanidine standard (Jicha et al., 2016) at the Oregon State University TRIGA reactor in the Cadmium-Lined In-Core Irradiation Tube. Single crystal fusion analyses were performed at the WiscAr laboratory at the University of Wisconsin-Madison using a 60-W CO_2 laser and a Noblesse multicollector mass spectrometer (Jicha et al., 2016). Full analytical data are reported in Supporting Information S1. Photographs of sampled stratigraphic units (SUs) for $^{40}Ar/^{39}Ar$ dating are provided in Supporting Information S1.

2.2. Electron Microprobe Analyses

Major oxides of glasses were analyzed at the CNR-IGAG (Istituto di Geologia Ambientale e Geoingegneria) di Roma, with a Cameca SX50 electron microprobe equipped with five wavelength dispersive spectrometers
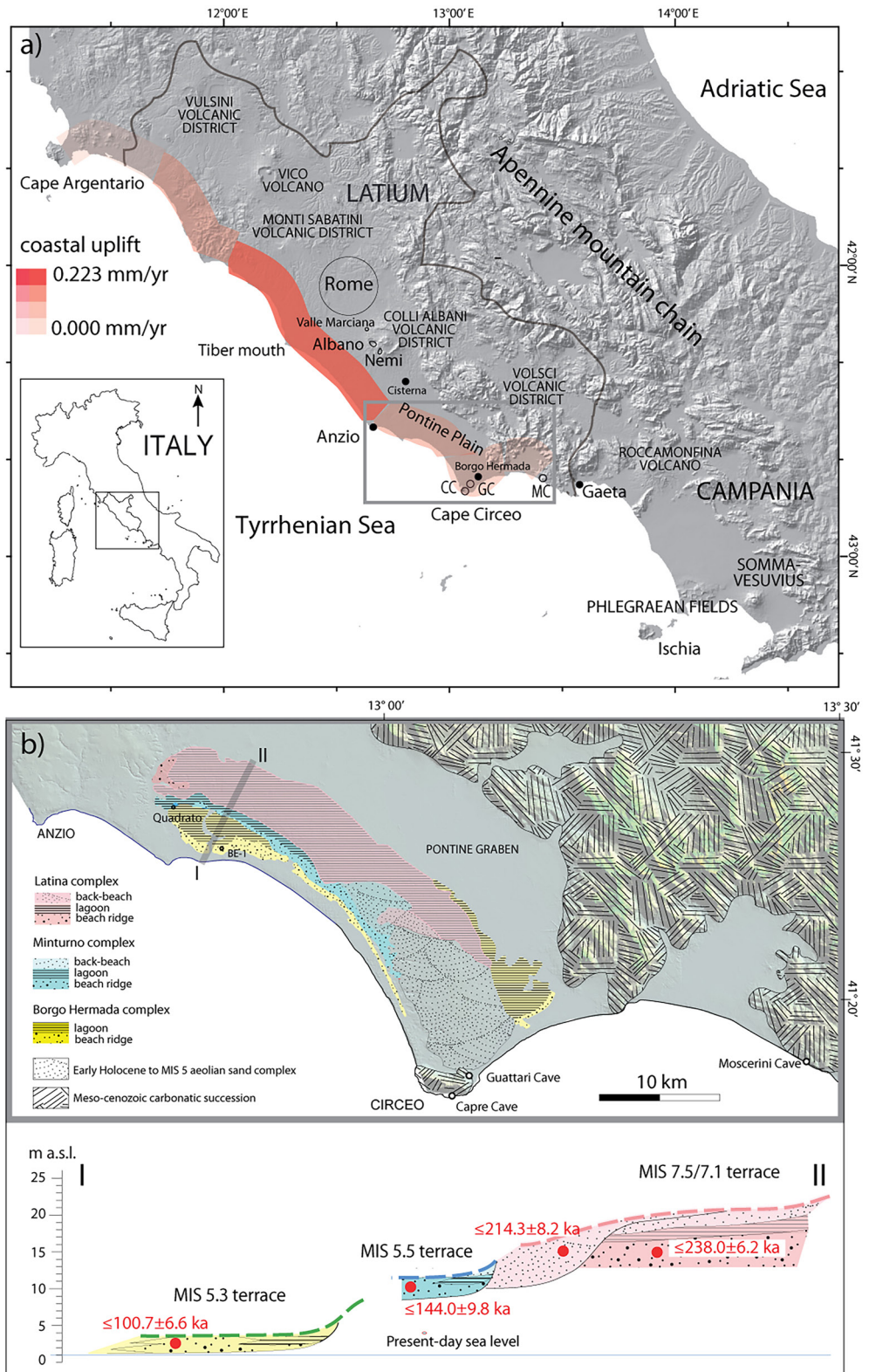
Figure 1. (a) Location map of the central Tyrrhenian Sea margin of Italy, showing the tectonic uplift rates affecting the coastal sector. (b) Morpho-structural sketch-map of the investigated coastal region, showing the age constraints to the suite of marine terraces reconstructed by Marra et al. (2023) in the tract between Capes Anzio and Circeo (≤ symbol indicates maximum ages derived from detrital sanidine dating method; see text for explanation). Background DEM image: TINITALY/01 square WA 6570, used with permission of the Istituto Nazionale di Geofisica e Vulcanologia, Rome.

(WDS). Quantitative analyses were performed using 15 kV accelerating voltage and 15 nA beam current. The standards we employed include metals for Mn and Cr, jadeite for Na, wollastonite for Si and Ca, orthoclase for K, corundum for Al, magnetite for Fe, rutile for Ti, periclase for Mg, F-apatite for P, phlogopite for F, potassium chloride for Cl, barite for Ba and S, and celestine for Sr. Counting times for all elements were 20 s on peak and half time on both backgrounds. Light elements (Na, K) were counted first to prevent loss by volatilization. The Peak-to-Background Area Percent correction method was used. Minerals were analyzed using a beam diameter of 1–5 μm, whereas to minimize alkali loss during glass analysis, the beam was defocused to 15 μm. In order to evaluate the accuracy of the analyses, repeated analyses of three international secondary standard (Kakanui augite, Iceladic Bir-1, and rhyolite RLS132 glasses from USGS) were made prior to any series of measurements. The mean precision from the standard value was about 1% for SiO_2, 2% for Al_2O_3, 5% for K_2O, CaO, and FeO, and 8%–10% for other elements. Moreover, the analytical precision (2σ error) is $\leq$1% for elements in the concentration range >10 wt% oxide, 5% for elements in the range 2–10 wt% oxide, and better than 10% for elements in the range 0.5–2 wt% oxide. From chemical analyses, the volatile ($H_2O \pm CO_2$) contents of glasses were estimated according to the by-difference method (Devine et al., 1995; Humphreys et al., 2006).

3. Cave Stratigraphy and Relationships With the Local Sea-Level Indicators

3.1. Sea-Level Indicators

A series of caves occur at elevations from ranging 5–10 m above sea level (a.s.l.) in the pre-Quaternary limestone reefs of the Tyrrhenian Sea coast in southern Latium (Figure 1). Different sets of sea-level markers, represented by tidal notches, horizontal stripes of *Lithofaga* burrows, and characteristic bioclastic beach deposits ("panchina"), also occur within these caves. The occurrence of "Senegalese fauna," including the most characteristic gastropod species *Strombus bubonius* (=*Tetystrombus latus*), in the beach deposits is considered distinctive of the MIS 5.5 highstand (Antonioli et al., 1999; Ferranti et al., 2006; Hearty & Dai-Pra, 1986; Nisi et al., 2003). The above-mentioned literature has considered this coastal region tectonically stable, substantially based on the reconstruction of the MIS 5.5 paleo-sea level and the comparison with its elevation throughout the Tyrrhenian Sea coast (Ferranti et al., 2006; Nisi et al., 2003) and in the whole Mediterranean Sea (Antonioli et al., 2018). These works have shown that the MIS 5.5 paleo-sea level is raised up to +35 m in the central portion of the coastal sectors comprised between Cape Argentario and Cape Circeo, and it descends down to ca. +4 at its margins. The uplifted coastal sector corresponds to the area where the Quaternary volcanic districts of central Italy are located (see Figure 1a). Cape Circeo is located at the southern end of the bulged coastal area where elevation of the MIS 5.5 sea level progressively descends from +9.5 to +4 m in few kilometers (Nisi et al., 2003). Other work has shown that the average elevation of the MIS 5.5 sea level throughout the most stable Mediterranean regions (including the Tyrrhenian Sea coast) is +8 m (Antonioli et al., 2018, and ref. therein). This fact excludes that the coastal sector investigated in our work was affected by any significant differential tectonic/glacio-isostatic movement with respect to the Mediterranean region in the last 125 kyr.

For this reason, and considering the low latitude of the region, GIA effects are not considered to be substantial in this region (e.g., Stocchi et al., 2018).

However, a moderate uplift rate in the order of 0.1 mm/year in the interval 250–80 ka was assessed based on elevation of the MIS 7.5 thorough MIS 5.3 marine terraces in the coastal sector between Cape Circeo and Cape Anzio (Marra et al., 2023; see Figure 1a).

The MIS 5.5 sea level is marked by a clearly discernible tidal notch, which occurs at progressively lower elevations from ~9.5 to ~4.5 m a.s.l. at several locations along the coast between Circeo and Gaeta promontories (Antonioli et al., 1999; Ferranti et al., 2006; Nisi et al., 2003). This tidal notch is associated with *Lithofaga* sp. burrows and *S. bubonius*-bearing beach deposits (Durante & Settepassi, 1974; Hearty & Dai-Pra, 1986). A well-preserved marine terrace at 11–14 m a.s.l., marking the MIS 5.5 transgressive cycle in the coastal sector between Anzio and Cape Circeo (Minturno pedo-morpho-stratigraphic complex; Marra et al., 2023; Sevink et al., 1982), is associated with the notch at 9.5 m (Figure 1).

A lower set of sea-level indicators occurring at 1.5–3 m a.s.l. in this coastal reach has been reported in the local literature (Blanc & Segre, 1953; Durante & Settepassi, 1976–1977; Zei, 1979), which has been neglected by most subsequent studies. A tidal notch situated at 2–3 m a.s.l. in the Circeo area (Durante & Settepassi, 1976–1977), though it is less prominent than the 9.5 m one, also contains well-preserved remains of cemented beach sand sediments
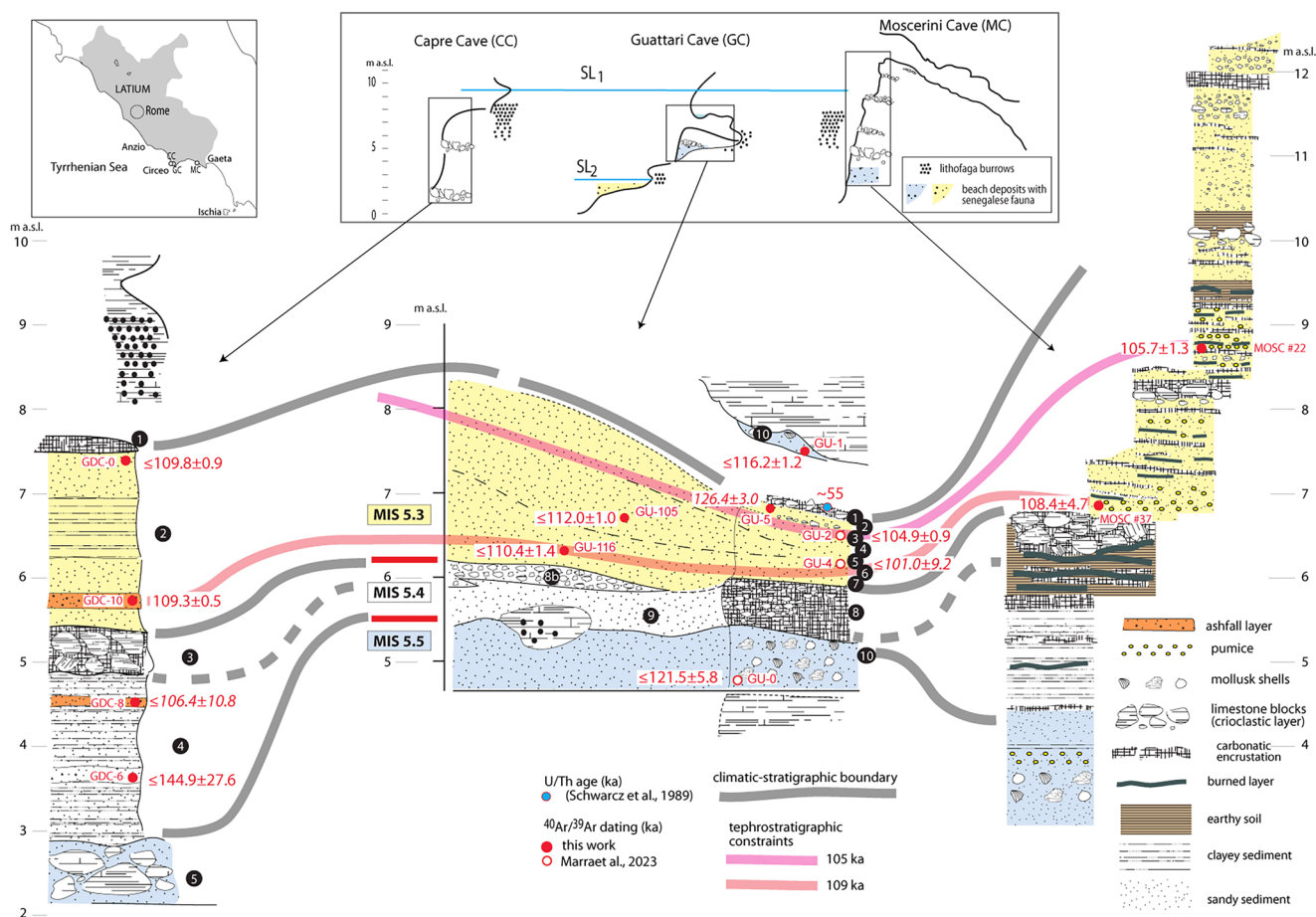
Figure 2. Geologic sketches of Capre, Guattari, and Moscerini Caves, showing the stratigraphic units and the $^{40}Ar/^{39}Ar$ geochronologic constraints achieved in this and previous (Marra et al., 2023) studies. The symbol ≤ indicates that the youngest crystal population in the sample provides a maximum age for the deposit. In italic: ages affected by large uncertainties that are discarded in favor of stratigraphically consistent, more precise ones.

and biogenic limestone embedding a "reduced" Senegalese fauna (i.e., lacking *Strombus*; Gignoux, 1913). These deposits form a suite of low marine terraces associated with remains of an abrasion platform situated at 1.5–2 m a.s.l. at Cape Circeo (Blanc & Segre, 1953; Durante & Settepassi, 1974, 1976–1977; Zei, 1979). These terraces correlate with another transgressive pedo-morpho-stratigraphic complex (Borgo Hermada complex; Marra et al., 2023; Sevink et al., 1982) situated at 3–5 m a.s.l. One sediment sample collected in the beach ridge sand deposit of the Borgo Hermada complex in the coast 30 km northwest of Cape Circeo yielded a maximum age of 100.7 ± 6.6 ka (Marra et al., 2023; Figure 1), suggesting correlation with MIS 5.3 highstand.

3.2. Guattari Cave Stratigraphy

GC is located at ca. 6 m a.s.l. at the foot of the eastern slope of Cape Circeo and is formed by a Mesozoic-Cenozoic limestone succession, ca. 300 m inland from the present coast (Figure 1). Marra, Rolfo, et al. (2020) identified 10 main SUs constituting the sedimentary fill of the external and atrial portion of the cave (SUs 0–10, Figure 2). A more detailed micromorphological study of the cave fill has been provided by Cremaschi et al. (2022). Here, the focus is on the SU 10 (subunit 1; Cremaschi et al., 2022) and on the overlying sand horizons constituting the SUs 7–2 (subunits 2–5; Cremaschi et al., 2022), which in previous studies (Blanc & Segre, 1953; Taschini, 1979) have been interpreted as "beach" and "dune" deposits, respectively. These two sets of sandy horizons are separated by a layer consisting of rubble with unsorted, subangular limestone clasts in a coarse sand matrix (SU 8, corresponding to subunit 2 base in Cremaschi et al. [2022], for which these authors suggested a cryo-clastic origin). This layer is only present in the interior of the cave and is exposed on the cave face where it is ca. 60 cm thick (Figure 2).

In order to provide age constraints to these sea-level indicators, we have ^{40}Ar/^{39}Ar dated single sanidine crystals extracted from four sandy sediment samples collected in different SUs of the cave fill (GU-1, GU-5, GU-105, and GU-116, Figure 2 and Figures S2 and S3 in Supporting Information S1). These four samples integrate previous age determinations on three samples dated by Marra et al. (2023) (GU-0, GU-2, and GU-4, Figure 2).

3.3. Capre Cave Stratigraphy

CC is located on the southernmost limestone reef of Cape Circeo, ca. 1 km southwest of MC, at ca. 7 m above the present coastline. Its sedimentary fill has been described by Blanc and Segre (1953) who recognized 14 SUs. We have distinguished 5 main SUs based on their paleoenvironmental context (Figure 2 and Figures S2–S4 in Supporting Information S1) and are described herein:

SU 5: Coarse conglomerate made up of well-rounded, dm- to m-sized blocks of limestone rock originated by wave action on the fallen cave vault's fragments.

SU 4: 1.5–2.0-m-thick suite of colluvial, dark reddish-brown sandy clay deposits with abundant, cm-sized limestone fragments and vertebrate bones.

Two samples for ^{40}Ar/^{39}Ar dating have been collected in this unit: a primary fallout layer (GDC-8) and a sediment sample (GDC-6; Figure 2 and Figures S2–S4 in Supporting Information S1).

SU 3: Large, subangular limestone blocks in reddish-brown sand matrix, originated by roof spall. Like similar rockfall horizons occurring at MC (Stiner & Kuhn, 1992), this layer was interpreted as a cryo-clastic conglomerate (Blanc & Segre, 1953; i.e., originated by water freezing within the fractures affecting the cave vault).

SU 2: 2.5-m-thick succession of reddish-brown loamy sand deposits.

SU 1: 10–20-cm-thick horizon of cm-sized, subangular limestone clasts, strongly cemented by carbonate. One primary tephra layer and one sediments sample have been collected in this unit for ^{40}Ar/^{39}Ar dating (GDC-10, GDC-0, Figure 2 and Figures S2–S4 in Supporting Information S1).

3.4. Moscerini Cave Stratigraphy

MC opens at ca. 5 m a.s.l. on a tall limestone reef along the coast of southern Latium, ca. 32 km east of Cape Circeo. New sedimentologic investigations have not been possible due to a landslide that blocked the cave entrance several years ago. A detailed reconstruction of its sedimentary fill has been performed by Marra, Rolfo, et al. (2020) based on an unpublished, annotated stratigraphic log by the geologist Aldo Segre who participated in the 1949 excavations. Moreover, a number of pumice clasts intercalated within the sand deposit forming the cave fill, stored at the IIPU repository in Anagni along with other archeological materials recovered during the excavations, were analyzed (Marra, Rolfo, et al., 2020; Villa et al., 2020). Geochemical analyses on five pumice clasts were provided by Marra, Rolfo, et al. (2020), while ^{40}Ar/^{39}Ar dating and SEM analysis of two of these pumice clasts (samples MOSC #37 and MOSC #22; Figure 2 and Figures S2–S5 in Supporting Information S1) have been performed for the present study.

A beach deposit with mollusk shells (including *S. bubonius*) occurs at the base of the sedimentary fill of MC (Stiner & Kuhn, 1992), followed by a succession of continental deposits, ca. 8 m thick, including cm- to dm-thick sandy and clay layers, carbon-rich (burned) layers, and stalagmitic crusts (Figure 2 and Figures S2–S5 in Supporting Information S1). Four layers consisting of fallen blocks of limestone rock (talus) are intercalated at different elevations in the succession, which are interpreted by Segre as cryo-clastic conglomerate, possibly corresponding to the occurrence of cold periods. A series of *Lithofaga* burrows was also described to occur on the outer, northern wall of the cave, approximately between 5 and 8 m a.s.l. (Stiner & Kuhn, 1992).

4. Results

4.1. ^{40}Ar/^{39}Ar Analysis

Results of the ^{40}Ar/^{39}Ar analyses on the 10 samples dated in this work are summarized in Table 1 where ages of 5 samples dated by Marra et al. (2023) are also reported. Results are also presented as age probability diagrams

Table 1
Summary of $^{40}Ar/^{39}Ar$ Data

Sample	Volcanic deposit	Average K/Ca	N	MSWD	Weighted mean age (ka)	$\pm 2\sigma$	
GU-4	Reworked	10.9	3/25	0.08	101.0	±9.2	[1]
BE-1	Reworked	9.7	4/28	1.69	100.7	±6.6	[1]
GU-2	Reworked	16.2	9/30	1.07	104.9	±0.9	[1]
MOSC-22	Pumice	8.5	23/23	0.94	105.7	±1.3	This work
GDC-8	Fallout	18.7	2/23	0.67	106.4	±10.8	This work
MOSC-37	Pumice	3.5	28/29	0.92	108.4	±4.7	This work
GDC-10	Fallout	12.1	21/29	0.92	109.3	±0.5	This work
GDC-0	Reworked	12.9	20/29	1.21	109.8	±0.9	This work
GU-116	Reworked	12.5	12/30	0.68	110.4	±1.4	This work
GU-105	Reworked	11.9	13/29	1.01	112.0	±1.0	This work
GU-1	Reworked	20.6	11/27	1.13	116.2	±1.2	This work
GU-0	Reworked	30.1	3/52	0.31	121.5	±5.8	[1]
GU-5	Reworked	7.0	9/44	0.65	126.4	±3.0	This work
QUA	Reworked	24.0	2/26	0.11	144.0	±9.8	[1]
GDC-6	Reworked	28.7	1/19	8,397.04	144.9	±27.6	This work

Note. Ages calculated relative to 1.1864 Ma Alder Creek sanidine (Jicha et al., 2016). N = number of dates used in weighted mean/total number of single crystal fusion dates. $\pm 2\sigma$ = analytical uncertainty plus J uncertainty. MSWD = mean square of weighted deviates. See Supporting Information S1 for complete data sets. [1] Ages performed by Marra et al. (2023).

in Figures S1 and S2 in Supporting Information S1, along with a detailed discussion of the age data. Maximum depositional ages were calculated based on the youngest date or youngest population of dates for each sample. There are two exceptions to this age calculation criteria. The youngest grains in samples GU-0 and GDC-10 have much lower radiogenic Ar yields (<25% $^{40}Ar^*$) than the rest of the grains in the sample, indicative of alteration or fast pathways. Thus, the next oldest population of grain dates with higher radiogenic Ar was used to calculate the age of the sample.

4.2. Petrographic and Geochemical Analyses

Under an optical microscope, the MC pumice clasts MOSC-37 and MOSC-22 display a glassy, vesicular texture and appear poorly porphyritic with a total phenocryst content ≤2 vol% (Figures 3a–3d). In particular, the MOSC-37 pumice clast shows a higher amount of vesicles (Figure 3a) and mineral clusters in which alkali-feldspar, plagioclase, biotite, Ti-magnetite, and titanite occur (Figures 3c and 3d). The MOSC-22 pumice clast has fewer vesicles (Figure 3b) with rare feldspars.

The glasses from the two samples share a similar trachytic composition, almost indistinguishable on a Total Alkali-Silica (TAS) diagram (Figure 3e). Nevertheless, they can be easily discriminated using other bivariate diagrams. The MOSC-37 glass is poor in CaO, MgO and TiO_2 compared to the MOSC-22 glass (Figure 3f). These glass compositions indicate that the parental magma of the 22 pumice clast is less differentiated with respect to that of MOSC-37 pumice clast, which underwent increased crystal fractionation of a Ti-bearing phase (Figure 3d). The different vesiculation patterns (Figures 3a and 3b) suggest, moreover, that the magmatic differentiation processes for each magma occurred at distinct pressure conditions. Specifically, the higher amount of $H_2O + CO_2$ (i.e., volatiles in Figure 3f) in the glasses, constrains the parental magma of the MOSC-22 scoria clasts to higher pressure.

Pumice samples MOSC-37 and MOSC-22 have an alkali-rich composition at the border between the phonolitic and trachytic fields in the TAS diagram (Figure 3e) which, combined with a $K_2O/Na_2O < 1$ and their mineralogical assemblage, matches the typical composition of the products of Ischia Island, as well as those of the early activity of the Phlegraean Fields. Marra, Rolfo, et al. (2020) found a good geochemical correspondence of MOSC-37 with tephra TM-33-1c/TM-33-2a dated to 118.2 ± 5.9 and 116.10 ± 5.8 ka, respectively, or with
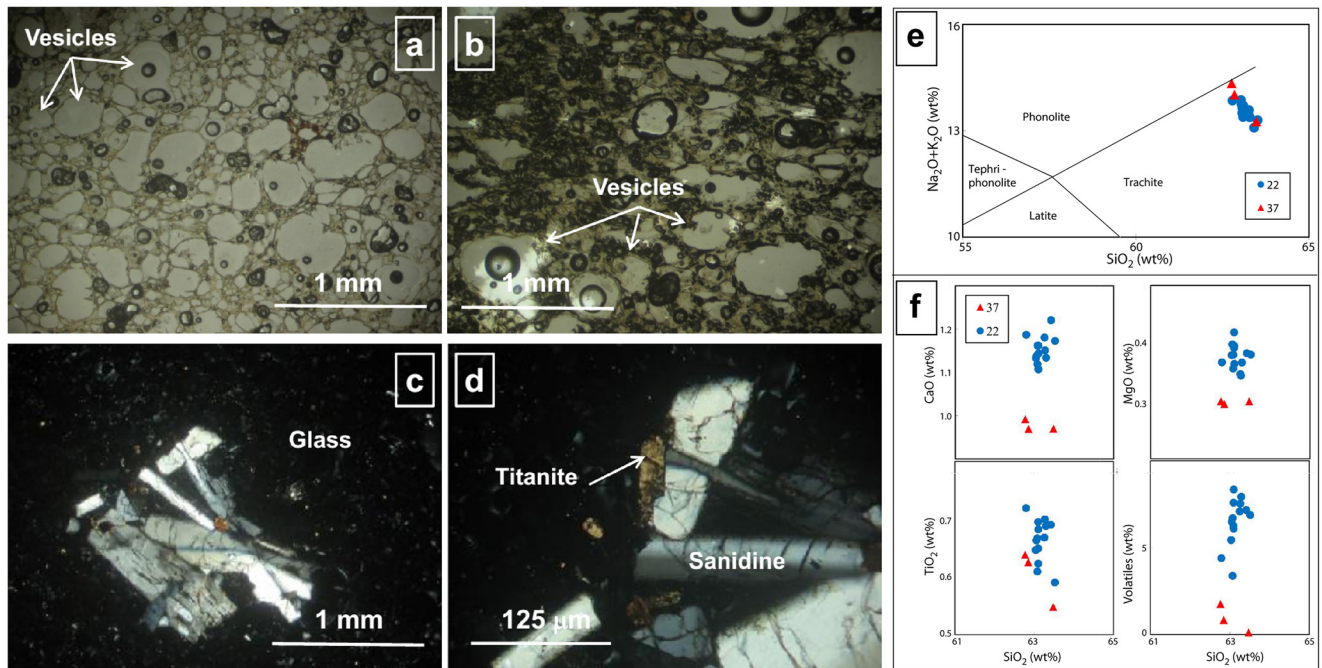
Figure 3. Photomicrographs ((a, b) plane-polarized light; (c, d) crossed nicols) of the MOSC-37 and MOSC-22 pumice clasts. Vesiculation pattern of the 37 pumice clast (a). Vesiculation pattern of the #22 pumice clast (b). Sanidine, plagioclase, biotite, Ti-magnetite, and titanite cluster in the MOSC-37 pumice clast (c). Detail of the mineral cluster showing the titanite (d). (e) Total alkali versus silica classification diagram of the glasses in the MOSC-37 and MOSC-22 pumice clasts. (f) CaO, MgO, TiO_2, and volatiles versus SiO_2 covariations for the glasses in the MOSC-37 and MOSC-22 pumice clasts. Volatiles (i.e., $H_2O + CO_2$) are estimated according to volatiles $= 100 - \Sigma EMPA_{total}$ equation.

the tephra TM-24-3, also found in Sulmona basin (POP2b; Giaccio et al., 2012) and dated to ~104.0 (Wulf et al., 2012). These distal tephra are correlated with two eruptive units from Ischia: Punta Imperatore and Mt. Sant'Angelo (Gillot et al., 1982; Poli et al., 1987). However, the only eruptive unit which has an age compatible with that of MOSC-37 and MOSC-22 is Monte Sant'Angelo, which has been determined based on the sedimentation rate of the lacustrine basin. In particular, a closer correspondence is observed with MOSC-22, whereas age of MOSC-37 matches that of the Phlegraean Fields' Maddaloni unit (Monaco et al., 2022; see Table 2).

5. Discussion

5.1. Age Constraints

The analyzed sand samples yielded widely dispersed crystal ages that are due to reworking or the incorporation of crystals from eroded volcanic deposits cropping out in the catchment basins of the rivers flowing in this coastal region. These crystals, both as loose particles or incorporated in sub-mm sized aggregates, were transported by rivers and sea currents and deposited in the coast-to-beach setting and successively accumulated as wind-blown deposits in the backbeach sector. Moreover, a minor contribution of primary volcanic airfall cannot be excluded as a source of the extracted crystals.

The youngest crystal populations in these sedimentary samples provide maximum ages (*terminus post quem*) on the time of deposition of the host sediment (Marra, Gaeta, et al., 2019). In order to provide age constraints on the MIS 5 sea levels, we have to consider the most recent volcanic activity in the interval 150–80 ka, which occurred in the volcanic districts of Latium and Campania (see Figure 1), with a particular focus on the Phlegraean Fields, which were the most active in this time span (e.g., Di Vito et al., 2008; Monaco et al., 2022). Precise $^{40}Ar/^{39}Ar$ dating of this eruptive activity was provided by Monaco et al. (2022), who distinguished five eruptive units: Maddaloni (109.3 ± 1.0 ka), Montemaoro (not dated), Cancello (102.5 ± 0.8 ka), Santa Lucia (101.2 ± 0.8 ka), and Triflisco (91.8 ± 1.2 ka; Table 2).

A slightly older activity is known from the tephrostratigraphic records of Lago Grande di Monticchio (Wulf et al., 2012), where two layers dated to 118.2 ± 5.9/116.10 ± 5.8 ka (TM-33-1c/TM-33-2a) and to ~104 ka

Table 2
Correlation Between the Known Volcanic Activity in the Time Span 150–70 ka and the Ages Yielded by the Primary and Detrital Samples Dated in This Work and in Marra et al. (2023) (Ages in ka; Uncertainties at 2σ)

			Sea-level indicators[this work, (4)]	
Colli Albani[1]	Phlegraean Fields: Ischia[2, 3]	Tephrostratigraphic record[2]	Primary	Detrital
Albano I **70 ± 1**				
	Triflisco **91.8 ± 1.2**			
Valle Marciana **100 ± 2**	Santa Lucia **101.2 ± 0.8**			BE-1 **100.7 ± 6.6**
	Cancello **102.5 ± 0.8**			
	Montemaoro/Mt. Sant'Angelo?	TM-24-23 *~104*	MOSC22 **105.7 ± 1.3**	GU-2 **104.9 ± 0.9**
	Maddaloni **109.3 ± 1.0**		MOSC37 **108.4 ± 4.7**	GDC-0 **109.8 ± 0.9**
			GDC-10 **109.3 ± 0.5**	GU-116 **110.4 ± 1.4**
				GU-105 **112.0 ± 1.0**
	Punta Imperatore?	TM-33-1c–TM-33-2a		GU-1 **116.2 ± 1.2**
		118.2 ± 5.9–116.10 ± 5.8		
				GU-0 **121.5 ± 5.8**
				GU-5 **126.4 ± 3**
Nemi II **142 ± 4**				QUA **144.0 ± 9.8**

Note. References: (1) Gaeta et al. (2016); (2) Wulf et al. (2012); (3) Monaco et al. (2022); (4) Marra et al. (2023). The value in italics means indirect dating and not with Ar/Ar method. The value in bold means dating with Ar/Ar method.

(TM-24-3) have been tentatively correlated with the Punta Imperatore and Mt. Sant'Angelo eruptive units of Ischia (Poli et al., 1987; Table 2).

Although closer to Cape Circeo, the Colli Albani volcanic district had only one minor eruption cycle between 143 and 70 ka, which occurred at the Valle Marciana maar at 100 ka (Marra, Gaeta, et al., 2016; Figure 1). It is unlikely that the products of the phreatomagmatic activity from this eruptive center reached the coast of southern Latium. In contrast, distal deposits of the 70 ± 1 ka Albano maar activity occur in the Pontine Plain at Borgo Hermada (Sevink et al., 2018), and near the town of Cisterna, north of Anzio (Gatta et al., 2017). Moreover, the abundant crystal dates of ca. 144 ka occurring in the samples collected in the deposits of the Minturno complex (including the Quadrato site, Figure 1) have been attributed to the latest cycle of activity at the Nemi crater (142 ± 4 ka; Gaeta et al., 2016), located northwest of the Pontine Plain (Figure 1).

Poorly constrained K/Ar ages ranging from 155 ± 24 to 53 ± 27 ka (Radicati di Brozolo et al., 1988) and one ^{40}Ar/^{39}Ar age of 148 ± 9 ka (Rouchon et al., 2008) have been reported for the late activity of Roccamonfina, which consist of small effusive episodes that likely could not comprise a significant component of the detrital record of the Latium coast. Similar considerations can be made for the phreatomagmatic activity that occurred between 150 and 70 ka at the Monti Sabatini, Vico and Vulsini district (Marra, Castellano, et al., 2020), located in northern Latium (Figure 1). Finally, no eruptive activity is documented at the Volsci district (including the Ernici volcanoes) after 231 ka (Marra, Cardello, et al., 2021).

An excellent correspondence between the ages of the samples dated for this study and in Marra et al. (2023) and those of known eruptive units is outlined in Table 2, with the only exception of the ages of 121.5 ± 5.8 and 126.4 ± 3 ka for GU-0 and GU-5, respectively. The paucity of crystal ages matching with MIS 5.5 highstand (i.e., ∼125 ka) has been noted and attributed to the lack of significant volcanic activity in this time period (Marra et al., 2023), as highlighted in Table 2, where no known eruptive unit of this age is reported. However, as for the case of sample QUA collected in the *Strombus*-bearing beach deposit of the Minturno complex, the lack of crystals of the abundant ca. 110 ka population occurring in the younger samples should be considered also to represent a "terminus ante quem" (i.e., minimum age), constraining the age between 110 and 144 ka.

The occurrence of two distinct eruption ages of ca. 109 and 105 ka framing the time of emplacement of the sedimentary fill of GC and MC is well supported by those of the primary deposits of Maddaloni and Montemaoro/ Mt. Sant'Angelo eruptive units (Table 2). Finally, the 100.7 ± 6.6 ka age of sample BE-1 provides a good
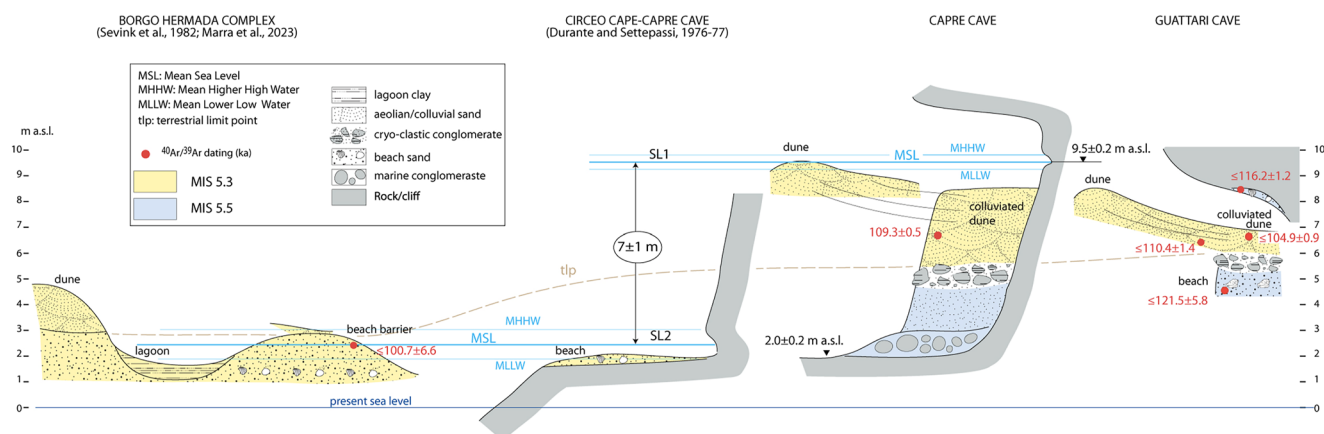
Figure 4. Geochronology and altimetry constraints to the sea-level indicators along the coast between Cape Circeo and Anzio. See text for further explanation.

correspondence with the Phlegraean Field's Cancello and Santa Lucia eruptive units (Table 2). The lack of 70 ka ages, despite the documented outcropping of the distal deposits of the 70 ± 1 ka eruption of the Albano crater (Sevink et al., 2018), may be regarded as providing a terminus ante quem for the sedimentary deposits of the Borgo Hermada complex. When the lack of crystals from the 91.8 ± 1.2 ka Triflisco eruption unit is also considered, a stricter constraint for MIS 5.3 ($>110 < 98$ ka) may be inferred for the Borgo Hermada marine terrace.

5.2. Ages of the Sea-Level Indicators at Cape Circeo

Figure 2 summarizes the chronostratigraphic correlations among the three sedimentary records that constitute the cave fill at CC, GC, and MC, based on the $^{40}Ar/^{39}Ar$ age constraints reported here and by Marra et al. (2023).

Two main sedimentary horizons, separated by a layer of fallen blocks, are recognized in each one of these caves. The lower horizon is made up of marine deposits, represented at GC and MC by a *S. bubonius*-bearing, biodetritic conglomerate, while at CC large rounded blocks of the cave wall rock are associated with *Lithofaga* burrows and a tidal notch, evidence for a marine transgression with a maximum sea level at ca. 9.5 m a.s.l.

Two samples of detrital sanidine extracted from the biodetritic deposit occurring at the base of the cave fill and within the cracks of the cave vault at GC (SU 10) yielded ages of 121 ± 5 and 116 ± 1 ka, respectively.

A 1–1.5-m-thick succession of loamy sand deposits of possible colluvial origin overly the marine horizon at MC and CC, while the layer of coarse limestone fragments rests directly on the bioclastic conglomerate at GC (Cremaschi et al., 2022). A variably thick suite of sand horizons occurs above the cryo-clastic layer in all the caves. According to Cremaschi et al. (2022), at GC, these sand horizons are distinguished between a lower portion representing the outcome of aeolian sand being blown into the cave from the backline dunes (subunits 2A–C, corresponding to SUs 7–6 in Figure 2) and an upper portion (subunits 3A–B and 5, corresponding to SUs 5–2 in Figure 2) for which colluvial processes (i.e., solifluction) are suggested as the main sediment transport mechanism.

Detrital sanidine $^{40}Ar/^{39}Ar$ maximum ages achieved at GC, combined with numerical ages of primary volcanic deposits intercalated in the equivalent stratigraphic horizons at CC and MC, constrain the age of deposition of these suites of sand horizons to the interval 110–105 ka (Figure 2).

Geochronological constraints provided here highlight that the sedimentary processes causing the filling of the caves are confined strictly within periods of high sea level, namely MIS 5.5 (125–119 ka) and MIS 5.3 (108–100 ka), while periods of sea-level fall correspond to sedimentary hiata, marked by emplacement of cryo-clastic layers (see Figure 4). Moreover, no ages younger than 126 ka occur in sample GU-5 collected at the very top of the sand succession within GC (Gs2 in Figure 4d), where a thin layer of small limestone blocks (Gb2 in Figure 4d) possibly correlating with the MIS 5.2 cold phase occurs. This suggests that no outer input, either aeolian or colluvial, reached the interior of the cave after 105 ka, but only detrital input from the cave ceiling and walls which reworked the beach deposit that filled the cave during MIS 5.5 highstand. Similar considerations can be inferred at CC, where no crystal ages younger than 109 ka occur in the uppermost portion of the sedimentary fill of the cave (Figure 4d).

These observations suggest a near-coast environment for the three similar sand packages, corresponding to a beach and backbeach settings, respectively, consistent with the occurrence of two sets of sea-level markers at ca.

9.5 and 2.5 m a.s.l. in this coastal region (Antonioli et al., 1999; Durante & Settepassi, 1974, 1976–1977; Ferranti et al., 2006; Nisi et al., 2003; Zei, 1979).

We note that the wind-blown deposits in a backbeach setting may occur up to several meters above sea level, but we use the precise sea-level markers from previous studies, represented by the lower tidal notch and the associated beach deposits occurring at ∼2.5 m a.s.l., to pinpoint the paleo-sea-level elevation, and we use the $^{40}Ar/^{39}Ar$ age constraints on the aeolian sediments of the cave fill to date them at 110–105 ka. Moreover, we correlate these backbeach deposits, the tidal notch, and the associated biodetritic conglomerate with the Borgo Hermada complex marine terrace, which occurs at 3–5 m a.s.l. and is dated at 100.7 ± 6.6 ka. Although this is an indirect age assessment, we believe that the considerations above represent a strong supporting framework for a MIS 5.3 sea level at ca. 2.5 m in this coastal reach, which requires further study to ascertain its causes.

5.3. Sea-Level Assessment

There is a vast literature on the upper sea-level indicators occurring at Cape Circeo, considered distinctive of MIS 5.5 highstand, the elevation of which has been assessed at 9.6 ± 0.5 m a.s.l. at CC (Nisi et al., 2003, and ref. therein). Using a Leica FlexLine TS09 total station, we determined that the mid-point of this well-marked tidal notch has an elevation of 9.5 ± 0.2 m a.s.l. (Figure 4).

Regarding the lower set of sea-level indicators, our aim is a preliminary assessment to compare with the established MIS 5.5 paleo-sea level. The tidal notch and the associated bioclastic conglomerate described by Durante and Settepassi (1976–1977) occur at an elevation between 2 and 3 m a.s.l. along the steep sea cliff at Cape Circeo (Figure 4). At CC, we have measured with the total station the elevation of the upper limit of the abrasion platform at the foot of a poorly preserved tidal notch at 2.0 ± 0.2 m a.s.l.

While a dedicated study, including GPS/RTK measurements (see Marra, Florindo, et al., 2016, for this methodology), is ongoing and will provide more precise assessment, we use this elevation in combination with that of the adjacent marine terrace of Borgo Hermada complex (Sevink et al., 1982), which has been dated at 100.7 ± 6.6 (Marra et al., 2023). Here, we have measured at 3 m with a portable GPS equipment (error ± 1 m) the elevation at which the regressive dune deposit oversteps the beach ridge (Figure 4).

Finally, we use the average elevation of the base of the colluviated dune deposits dated at 110–105 ka in GC and GG, measured with the total station at 6.0 (± 0.2) and 5.5 (± 0.2) m, respectively, as a further terrestrial limit point (e.g., Rovere et al., 2016) for the corresponding paleo-sea level (Figure 4).

Following Rovere et al. (2016), we use a conservative value of 2.5 ± 0.5 m for the elevation of the lower paleo-sea level (SL2, Figure 4), based on assessment of a Mean Sea Level corresponding to the mid-point of the tidal notch and Mean Higher High/Lower Low Water boundaries corresponding to the width of the notch (Figure 4). Using the same method, we assess the upper paleo-sea level (SL1) at 9.5 ± 0.3 m a.s.l.

We emphasize that the aim of this study is to demonstrate a notably higher elevation for the MIS 5.3 sea level compared to the value of −20/−25 m a.s.l. established by regression formulas (e.g., Rohling et al., 2009). According to the assumed value of +8 m for the MIS 5.5 sea level in the Mediterranean region (Antonioli et al., 2018), the MIS 5.3 sea level at Cape Circeo should occur approximately 30 m (8 + 20/25) below the tidal notch of CC, which we have determined to be at an elevation of 9.5 ± 0.3 m a.s.l. This means that the MIS 5.3 sea level should be roughly 20 m below the present sea level.

However, the set of lower sea-level indicators that we have analyzed provide a paleo-sea level at an elevation of 2.5 ± 0.5 m a.s.l., only 7 ± 1 m below the MIS 5.5 paleo-sea level. If we assume this as the MIS 5.3 sea level, it dramatically conflicts with global estimations (e.g., Rohling et al., 2009), even when accounting for potential errors in its assessment.

We note that the elevation of the MIS 5.5 sea level at Cape Circeo, which we have determined to be at 9.5 ± 0.3 m a.s.l., is only ∼1.5 m higher than the expected elevation in the Mediterranean region (i.e., ∼8 m; Antonioli et al., 2018). This suggests the absence of significant tectonic and isostatic effects in the coastal region. Therefore, it is unlikely that significant GIA effects on the MIS 5.3 sea level need to be considered, as it is expected also based on the latitude of this region (e.g., Stocchi et al., 2018). Future dedicated studies may help clarifying the possible role of GIA.
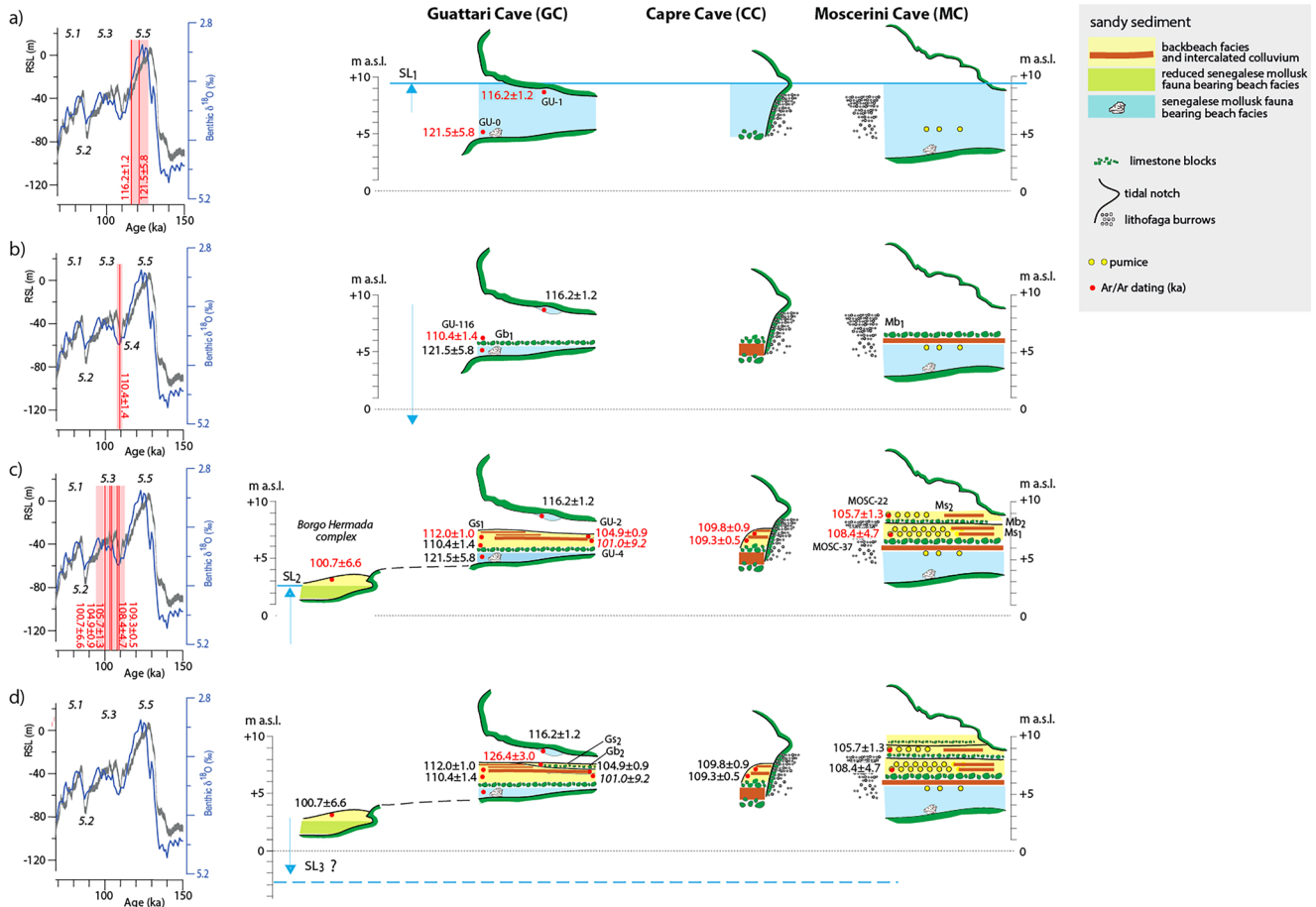
Figure 5. Reconstructed relative sea-level (RSL) elevations during Marine Isotope Stage (MIS) 5, based on sea-level indicators and their $^{40}Ar/^{39}Ar$ age constraints determined at Capre (CC), Guattari (GC), and Moscerini (MC) caves. $\delta^{18}O$ record by Lisiecki and Raymo (2005) and RSL curve by Grant et al. (2014) are reported for comparison.

5.4. Reconstructed Sea-Level History

Based on the detailed sedimentary record of GC, integrated by the chronostratigraphic constraints from CC and MC on the equivalent stratigraphic horizons discussed above, we hereby propose a reconstruction of the sea-level history during MIS 5.5–MIS 5.3 interval, as summarized in Figure 5.

An $^{40}Ar/^{39}Ar$ age of 116.2 ± 1.2 ka yielded by sample GU-1, collected from a patch of marine sand cemented to the GC ceiling at ∼ 7.50 m a.s.l. (Figure 2 and Figures S2 and S3 in Supporting Information S1), combined with the 121.5 ± 5.8 ka age of sample GU-0 collected at ∼ 5 m a.s.l. from a *S. bubonius*-bearing conglomerate, correlates well with the MIS 5.5 highstand and its associated 9.5 m a.s.l. tidal notch and *Lithophaga* burrows occurring along the Circeo coast.

The topographic and sedimentologic context of these ages, as well as *Lithophaga* burrows situated on the bottom part of the outer cave wall, show that the cave was inundated by the sea and filled by marine sediments during MIS 5.5 (Figure 5a), also suggesting that sea level remained as high as 7.5 m until 116.2 ± 1.2 ka (Figure 5a), consistent with data from other regions of the world (e.g., California, Hawaii, Bermuda, and Cuba; Muhs et al., 2002, 2011, 2017, 2020). However, this observation is not necessarily at odds with other inferences on a rapid sea-level drop since 122 ka (e.g., Bini et al., 2020) when the hypothesis on the occurrence of a second eustatic pulse during MIS 5.5 at ca. 119 ka (e.g., O'Leary et al., 2013) is considered.

The regressive phase following MIS 5.5 led to the sea-level lowstand of the glacial period during MIS 5.4, which fostered the erosion of the MIS 5.5 beach deposits that had filled the caves. This phase caused the emplacement of a horizon of coarse blocks derived from roof-spall of the cave ceiling/walls (Mb₁ in Figure 5b) which could

represent a phase of freeze-and-thaw and cryo-clastic deposition. The maximum age of 110.4 ± 1.4 ka yielded by sample GU-116, collected slightly above layer Gb1 at GC in sandy sediments, matches the age of the MIS 5.4 lowstand (Figure 5b) and supports this interpretation.

At MC, two samples of pumice clasts included in sandy sediments (Marra, Rolfo, et al., 2020) situated at 7.0 and 9.0 m a.s.l. are ^{40}Ar/^{39}Ar dated here to 108.4 ± 4.7 and 105.7 ± 1.3 ka (Figure 5c). Strict stratigraphic considerations suggest that these dates should indicate the maximum age of the layer because the pumices are considered to be reworked. However, the petrographic/geochemical characteristics of the two dated pumice clasts are different (Figures 3a–3d) and can be ascribed to two distinct, successive eruptions. The fact that the ages of the samples are in sequence within the stratigraphic succession suggests that their position is subprimary (i.e., slightly reworked soon after deposition) and that their age broadly corresponds to the age of the sediment. The ages obtained from these sediments provide a likely correlation with MIS 5.3 (Figure 5c). These MC deposits may be correlated with the broadly similar GC sediments (SUs 7–2) sampled by GU-116, GU-105, GU-5, GU-4, and GU-2 (Gs₁ in Figure 5c), overlying the MIS 5.4 limestone blocks layer. The ^{40}Ar/^{39}Ar age of 101.0 ± 9.2 of the lowest sample GU-4 has a large uncertainty but is superseded by the well-constrained ages of 110.4 ± 1.4 and 112.0 ± 1.0 ka yielded by samples GU-116 and GU-105. In contrast, the age of 104.0 ± 0.9 ka yielded by sample GU-2 is statistically distinct and younger. Consistent with indications from MC, where MOSC-37 and MOSC-22 yielded ages of 108.4 ± 4.7 and 105.7 ± 1.3 ka, ages of samples GU-116, GU-105, and GU-2 support an interpretation that the sand successions at MC and GC were emplaced from 110 ka through 105 ka, during the MIS 5.3 highstand (Figure 5c). The age of 109.3 ± 0.5 ka yielded by the primary fallout layer (sample GDC-10) collected at the base of the stratigraphically equivalent sand package (U2 in Figure 2) overlying the cryo-clastic horizon at CC further supports the inference that the upper suite of sand horizons was emplaced in a backbeach context during MIS 5.3 sea-level rise. According to micromorphological analysis in Cremaschi et al. (2022), the lower part of these sediments derives from the reworking of dunes and includes fine colluvium indicating active hillslope processes under humid conditions, consistent with their age corresponding to the initial stage of MIS 5.3. The geographic position along the coast and the elevation between 5.5 and 7 m a.s.l. of these backbeach sand horizons indicate a correlation with the suite of beach ridge deposits of the Borgo Hermada complex, occurring at 3–5 m a.s.l. in the coast between Capes Circeo and Anzio, dated at 100.7 ± 6.6 ka by Marra et al. (2023). This beach to backbeach morpho-stratigraphic context can be readily associated with the lower tidal notch occurring in the coastal sector near GC (Durante & Settepassi, 1976–1977; Zei, 1979), setting the local maximum MIS 5.3 local sea level at ~2.5 m a.s.l. (SL₂ in Figure 5c).

6. Conclusions

Results of this study constrain the sedimentary processes causing the filling of the costal caves of Guattari, Capre, and Moscerini within two intervals: 121–116 and 110–105 ka. Such intervals correspond to periods of high sea level, while periods of sea-level fall correspond to sedimentary hiata, marked by emplacement of cryo-clastic layers. This chronologic framework, combined with the sedimentologic features of the deposits, points to the evidence for a near-coast environment associated with the two sand packages, corresponding to a beach and a backbeach context, respectively. In addition, the geographic context and the elevation of these sand packages offer straightforward correlation with two sets of sea-level markers occurring at ca. 9.5 and 2.5 m a.s.l., as well as with two marine terraces occurring at ca. 11–14 and 3–5 m a.s.l. in this coastal region. Therefore, the ^{40}Ar/^{39}Ar age constraints to these sand packages, including the beach ridge deposit of the Borgo Hermada complex (Marra et al., 2023), suggest correlation for these paleo-coastlines with MIS 5.5 and MIS 5.3 highstands, respectively. We note that the maximum age of 100.7 ± 6.6 ka assigned to the beach ridge deposit of the Borgo Hermada complex, occurring ca. 3 m a.s.l., eliminates an interpretation that it may represent a feature developed during an hypothesized second sea-level oscillation of 119 ka during MIS 5.5 (e.g., O'Leary et al., 2013). In addition, we also exclude that the tidal notch at 2.5 ± 0.5 and the associated bioclastic marine conglomerate at CC may represent the sea-level markers of the 119 ka MIS 5.5 second peak. Consistently, the ^{40}Ar/^{39}Ar age constraints provided in this work on the marine sediments filling the cracks in the vault of GC indicate that the sea level was still ≥7.5 m at 116 ka, excluding that the paleo-sea level at 2.5 m may be 119 kyr old. We note that such duration of MIS 5.5 highstand is in line with estimation from other regions in the world (e.g., Muhs et al., 2011).

In contrast, while the elevation of MIS 5.5 paleo-sea level is consistent with the assumed tectonically stable setting of this coast and the estimation of a maximum sea level around 8 m in the Mediterranean region (e.g.,

Antonioli et al., 2018), a MIS 5.3 paleo-sea level at ca. 2.5 m a.s.l. is ca. 20 m higher with respect to the $\delta^{18}O$-derived predicted level (e.g., Rohling et al., 2009). We note that this datum is in line with reconstruction provided in Marra et al. (2023) for the coastal reach between Capes Circeo and Anzio, as well as with inferences from the paleo-Tiber delta, where three elevated marine terraces at 33–40, 24–28, and 11–17 m suggest a local relative sea-level (RSL) elevation at +2/−2 m a.s.l. for MIS 5.3 (Marra, Bahain, et al., 2019; Marra, Florindo, et al., 2016). These observations are more in line with a markedly different scenario presented for the MIS five interglacial in several studies of different regions of the world, including the Mediterranean Sea and the Pacific and Atlantic Oceans (e.g., Bermuda, Florida, California, and Grand Cayman), which call upon much higher sea levels (close to the present one) during MIS 5.3 and MIS 5.1 (e.g., Dorale et al., 2010; Medina-Elizalde, 2012; Muhs et al., 2002, 2011; Vicens et al., 2012; Wehmiller et al., 2004). While investigating the causes of the much higher MIS 5.3 and MIS 5.1 sea levels in these regions is beyond the scope of this study, our work should facilitate a thorough discussion on the reliability of the $\delta^{18}O$-based global sea-level estimations.

Conflict of Interest

The authors declare no conflicts of interest relevant to this study.

Data Availability Statement

Data sets for this research are available on the PANGAEA database (Florindo et al., 2023).

References

Antonioli, F., Ferranti, L., Stocchi, P., Deiana, G., Lo Presti, V., Furlani, S., et al. (2018). Morphometry and elevation of the Last Interglacial tidal notches in tectonically stable coasts of the Mediterranean Sea. *Earth-Science Reviews*, *185*, 600–623. https://doi.org/10.1016/j.earscirev.2018.06.017

Antonioli, F., Silenzi, S., Vittori, E., & Villani, M. (1999). Sea level changes and tectonic stability: Precise measurements in 3 coastlines of Italy considered stable during last 125 ky. *Physics and Chemistry of the Earth*, *24*(4), 337–342. https://doi.org/10.1016/s1464-1895(99)00038-1

Bini, M., Zanchetta, G., Drysdale, R. N., Giaccio, B., Stocchi, P., Vacchi, M., et al. (2020). An end to the Last Interglacial highstand before 120 ka: Relative sea-level evidence from Infreschi Cave (southern Italy). *Quaternary Science Reviews*, *250*, 106658. https://doi.org/10.1016/j.quascirev.2020.106658

Blanc, A. C., & Segre, A. G. (1953). Le Quaternaire du Monte Circeo. *4e Congr. Internat. INQUA, Guide à l'excurs au M. Circé* (pp. 23–31).

Box, J. E., Hubbard, A., Bahr, D. B., Colgan, W. T., Fettweis, X., Mankoff, K. D., et al. (2022). Greenland ice sheet climate disequilibrium and committed sea-level rise. *Nature Climate Change*, *12*(9), 808–813. https://doi.org/10.1038/s41558-022-01441-2

Cremaschi, M., Nicosia, C., & Favero, M. (2022). Extreme diagenesis in the Late Pleistocene stratigraphic sequence of Grotta Guattari (central Italy) and its impact on the archaeological record. *Quaternary Science Reviews*, *298*, 107732. https://doi.org/10.1016/j.quascirev.2022.107732

Devine, J. D., Gardner, J. E., Brack, H. P., Layne, G. D., & Rutherford, M. J. (1995). Comparison of microanalytical methods for estimating H₂O contents of silicic volcanic glasses. *American Mineralogist*, *80*(3–4), 319–328. https://doi.org/10.2138/am-1995-3-413

Di Vito, M., Sulpizio, R., Zanchetta, G., & D'Orazio, M. (2008). The Late Pleistocene pyroclastic deposits of the Campanian Plain: New insights into the explosive activity of Neapolitan volcanoes. *Journal of Volcanology and Geothermal Research*, *177*(1), 19–48. https://doi.org/10.1016/j.jvolgeores.2007.11.019

Dorale, J. A., Onac, B. P., Fornòs, J. J., Ginés, J., Ginés, A., Tuccimei, P., & Peate, D. W. (2010). Sea-level highstand 81,000 years ago in Mallorca. *Science*, *327*(5967), 860–863. https://doi.org/10.1126/science.1181725

Durante, S., & Settepassi, F. (1974). Livelli marini e molluschi tirreniani alla Grotta delle Capre (Circeo). *Memorie Istituto di Paleontologia Umana*, *2*, 286–296.

Durante, S., & Settepassi, F. (1976–1977). Malacofauna e livelli marini tirreniani a Grotta Guattari, Monte Circeo (Latina). *Quaternaria*, *19*, 35–69.

Ferranti, L., Antonioli, F., Mauzc, B., Amorosi, A., Dai Pra, G., Mastronuzzi, G., et al. (2006). Markers of the Last Interglacial sea-level high stand along the coast of Italy: Tectonic implications. *Quaternary International*, *145/146*, 30–54. https://doi.org/10.1016/j.quaint.2005.07.009

Florindo, F., Marra, F., Gaeta, M., & Jicha, B. (2023). 40Ar/39Ar age constraints to MIS 5.5 and MIS 5.3 paleo-sea levels: Implications for global sea levels and ice-volume estimation [Dataset]. PANGAEA. https://doi.org/10.1594/PANGAEA.960617

Gaeta, M., Freda, C., Marra, F., Arienzo, I., Gozzi, F., Jicha, B., & Di Rocco, T. (2016). Paleozoic metasomatism at the origin of Mediterranean ultrapotassic magmas: Constraints from time-dependent geochemistry of Colli Albani volcanic products (central Italy). *Lithos*, *244*, 151–164. https://doi.org/10.1016/j.lithos.2015.11.034

Gatta, M., Giaccio, B., Marra, F., Rolfo, M. F., & Jicha, B. R. (2017). Trace-element fingerprinting of the 69–36 ka Colli Albani eruptive units: A preliminary dataset for archaeological and tephra studies in central-southern Italy. *Journal of Archaeological Science: Reports*, *16*, 330–340. https://doi.org/10.1016/j.jasrep.2017.10.007

Giaccio, B., Nomade, S., Wulf, S., Isaia, R., Sottili, G., Cavuoto, G., et al. (2012). The late MIS 5 Mediterranean tephra markers: A reappraisal from peninsular Italy terrestrial records. *Quaternary Science Reviews*, *56*, 31–45. https://doi.org/10.1016/j.quascirev.2012.09.009

Gignoux, M. (1913). Les formations marines pliocènes et quaternaires de l'Italie du sud etde la Sicile. *Annales de l'Université de Lyon (n.s.)*, *36*, 1–693.

Gillot, P. Y., Chiesa, S., Pasquare, G., & Vezzoli, L. (1982). <33.000 yr K/Ar dating of the volcano-tectonic horst of the isle of Ischia, Gulf of Naples. *Nature*, *299*(5880), 242–245. https://doi.org/10.1038/299242a0

Grant, K. M., Rohling, E. J., Bronk Ramsey, C., Cheng, H., Edwards, R. L., Florindo, F., et al. (2014). Sea-level variability over five glacial cycles. *Nature Communications*, *5*(1), 5076. https://doi.org/10.1038/ncomms6076

Hearty, P. J., & Dai-Pra, G. (1986). Aminostratigraphy of Quaternary marine deposits in the Lazio region of central Italy. In A. Ozer & C. Vita-Finzi (Eds.), *Dating Mediterranean shorelines, Zeitschrift Fuer Geomorphologie* (Vol. 62, pp. 131–140).

Humphreys, M. C. S., Kearns, S. L., & Blundy, J. D. (2006). SIMS investigation of electron-beam damage to hydrous, rhyolitic glasses: Implications for melt inclusion analysis. *American Mineralogist*, *91*(4), 667–679. https://doi.org/10.2138/am.2006.1936

Jicha, B. R., Singer, B. S., & Sobol, P. (2016). Re-evaluation of the ages of ^{40}Ar/^{39}Ar sanidine standards and supereruptions in the western U.S. using a Noblesse multi-collector mass spectrometer. *Chemical Geology*, *431*, 54–66. https://doi.org/10.1016/j.chemgeo.2016.03.024

Lisiecki, L. E., & Raymo, M. E. (2005). A Pliocene–Pleistocene stack of 57 globally distributed benthic δ^{18}O records. *Paleoceanography*, *20*, PA1003. https://doi.org/10.1029/2004PA001071

Marra, F., Bahain, J.-J., Jicha, B., Nomade, S., Palladino, D. M., Pereira, A., et al. (2019). Reconstruction of the MIS 5.5, 5.3 and 5.1 coastal terraces in Latium (central Italy): A re-evaluation of the sea-level history in the Mediterranean Sea during the Last Interglacial. *Quaternary International*, *525*, 54–77. https://doi.org/10.1016/j.quaint.2019.09.001

Marra, F., Cardello, L., Gaeta, M., Jicha, B., Montone, P., Niespolo, E., et al. (2021). The Volsci volcanic field (central Italy): An open window on continental subduction processes. *International Journal of Earth Sciences*, *110*(2), 689–718. https://doi.org/10.1007/s00531-021-01981-6

Marra, F., Castellano, C., Cucci, L., Florindo, F., Gaeta, M., Jicha, B., et al. (2020). Monti Sabatini and Colli Albani: The dormant twin volcanoes at the gates of Rome. *Scientific Reports*, *10*(1), 8666. https://doi.org/10.1038/s41598-020-65394-2

Marra, F., Florindo, F., Anzidei, M., & Sepe, V. (2016). Paleo-surfaces of glacio-eustatically forced aggradational successions in the coastal area of Rome: Assessing interplay between tectonics and sea-level during the last ten interglacials. *Quaternary Science Reviews*, *148*, 85–100. https://doi.org/10.1016/j.quascirev.2016.07.0032016

Marra, F., Gaeta, M., Giaccio, B., Jicha, B., Palladino, D., Polcari, M., et al. (2016). Assessing the volcanic hazard for Rome: ^{40}Ar/^{39}Ar and In-SAR constraints on the most recent eruptive activity and present-day uplift at Colli Albani Volcanic District. *Geophysical Research Letters*, *43*, 6898–6906. https://doi.org/10.1002/2016GL069518

Marra, F., Gaeta, M., Jicha, B. R., Nicosia, C., Tolomei, C., Ceruleo, P., et al. (2019). MIS 9 to MIS 5 terraces along the Tyrrhenian Sea coast of Latium (central Italy): Assessing interplay between sea-level oscillations and tectonic movements. *Geomorphology*, *346*, 106843. https://doi.org/10.1016/j.geomorph.2019.106843

Marra, F., Pereira, A., Boschian, G., & Nomade, S. (2021). MIS 13 and MIS 11 aggradational successions of the Paleo-Tiber delta: Geochronological constraints to sea-level fluctuations and to the Acheulean sites of Castel di Guido and Malagrotta (Rome, Italy). *Quaternary International*, *616*, 1–11. https://doi.org/10.1016/j.quaint.2021.12.016

Marra, F., Rolfo, F. M., Gaeta, M., & Florindo, F. (2020). Anomalous Last Interglacial Tyrrhenian Sea levels and Neanderthal settling at Guattari and Moscerini Caves (central Italy). *Scientific Reports*, *10*(1), 11929. https://doi.org/10.1038/s41598-020-68604-z

Marra, F., Sevink, J., Tolomei, C., Vannoli, P., Florindo, F., Jicha, B. R., & La Rosa, M. (2023). New age constraints on the MIS 9 through MIS 5.3 marine terraces of the Pontine Plain (central Italy) and implications for global sea levels. *Quaternary Science Reviews*, *300*, 107866. https://doi.org/10.1016/j.quascirev.2022.107866

Marra, F., Taddeucci, J., Freda, C., Marzocchi, W., & Scarlato, P. (2004). Recurrence of volcanic activity along the Roman Comagmatic Province (Tyrrhenian margin of Italy) and its tectonic significance. *Tectonics*, *23*, TC4013. https://doi.org/10.1029/2003TC001600

Medina-Elizalde, M. (2012). A compilation of coral sea-level benchmarks: Implications and new challenges. *Earth and Planetary Science Letters*, *362*, 310–318. https://doi.org/10.1016/j.epsl.2012.12.001

Monaco, L., Palladino, D. M., Albert, P. G., Arienzo, I., Conticelli, S., Di Vito, M., et al. (2022). Linking the Mediterranean MIS 5 tephra markers to Campi Flegrei (southern Italy) 109–92 ka explosive activity and refining the chronology of MIS 5c-d millennial-scale climate variability. *Global and Planetary Change*, *211*, 103785. https://doi.org/10.1016/j.gloplacha.2022.103785

Muhs, D. R., Schweig, E. S., Simmons, K. R., & Halley, R. B. (2017). Late Quaternary uplift along the North America–Caribbean plate boundary: Evidence from the sea level record of Guantanamo Bay, Cuba. *Quaternary Science Reviews*, *178*, 54–76. https://doi.org/10.1016/j.quascirev.2017.10.024

Muhs, D. R., Simmons, K. R., Meco, J., & Porat, N. (2015). Uranium-series ages of fossil corals from Mallorca, Spain: The "Neotyrrhenian" high stand of the Mediterranean Sea revisited. *Palaeogeography, Palaeoclimatology, Palaeoecology*, *438*, 408–424. https://doi.org/10.1016/j.palaeo.2015.06.043

Muhs, D. R., Simmons, K. R., Schumann, R. R., & Halley, R. B. (2011). Sea-level history of the past two interglacial periods: New evidence from U-series dating of reef corals from south Florida. *Quaternary Science Reviews*, *30*(5–6), 570–590. https://doi.org/10.1016/j.quascirev.2010.12.019

Muhs, D. R., Simmons, K. R., Schumann, R. R., Schweig, E. S., & Rowe, M. P. (2020). Testing glacial isostatic adjustment models of last-interglacial sea level history in the Bahamas and Bermuda. *Quaternary Science Reviews*, *233*, 106212. https://doi.org/10.1016/j.quascirev.2020.106212

Muhs, D. R., Simmons, K. R., & Steinke, B. (2002). Timing and warmth of the Last Interglacial period: New U-series evidence from Hawaii and Bermuda and a new fossil compilation for North America. *Quaternary Science Reviews*, *21*(12–13), 1355–1383. https://doi.org/10.1016/s0277-3791(01)00114-7

Muhs, D. R., Simmons, K. S., Schumann, R. R., Groves, L. T., Mitrovica, J. X., & Laurel, D. (2012). Sea-level history during the Last Interglacial complex on San Nicolas Island, California: Implications for glacial isostatic adjustment processes, paleozoogeography and tectonics. *Quaternary Science Reviews*, *37*, 1–25. https://doi.org/10.1016/j.quascirev.2012.01.010

Nisi, M. F., Antonioli, F., Dai Pra, G., Leoni, G., & Silenzi, S. (2003). Coastal deformation between the Versilia and the Garigliano plains (Italy) derived from the elevations of the Last Interglacial stage. *Journal of Quaternary Science*, *18*(8), 709–721. https://doi.org/10.1002/jqs.803

O'Leary, M. J., Hearty, P. J., Thompson, W. G., Raymo, M. E., Mitrovica, J. X., & Webster, J. M. (2013). Ice sheet collapse following a prolonged period of stable sea level during the Last Interglacial. *Nature Geoscience*, *6*(9), 796–800. https://doi.org/10.1038/ngeo1890

Pasquetti, F., Bini, M., Giaccio, B., Ratti, A., Vacchi, M., & Zanchetta, G. (2021). Chronology of the Mediterranean sea-level highstand during the Last Interglacial: A critical review of the U/Th-dated deposits. *Journal of Quaternary Science*, *36/7*(7), 1174–1189. https://doi.org/10.1002/jqs.3359

Peccerillo, A. (2017). *Plio-Quaternary volcanism in Italy—Petrology, geochemistry, geodynamics*. Springer.

Poli, S., Chiesa, S., Gillot, P.-Y., Gregnanin, A., & Guichard, F. (1987). Chemistry versus time in the volcanic complex of Ischia (Gulf of Naples, Italy): Evidence of successive magmatic cycles. *Contributions to Mineralogy and Petrology*, *95*(3), 322–335. https://doi.org/10.1007/bf00371846

Radicati di Brozolo, F., Di Girolamo, P., Turi, B., & Oddone, M. (1988). ^{40}Ar–^{39}Ar and K–Ar dating of K-rich rocks from the Roccamonfina Volcano, Roman comagmatic region, Italy. *Geochimica et Cosmochimica Acta*, *52*(6), 1435–1441. https://doi.org/10.1016/0016-7037(88)90213-x

Rohling, E. J., Grant, K., Bolshaw, M., Roberts, A. P., Siddall, M., Hemleben, C., & Kucera, M. (2009). Antarctic temperature and global sea level closely coupled over the past five glacial cycles. *Nature Geoscience*, *2*(7), 500–504. https://doi.org/10.1038/ngeo557

Rouchon, V., Gillot, P. Y., Quidelleur, X., Chiesa, S., & Floris, B. (2008). Temporal evolution of the Roccamonfina volcanic complex (Pleistocene), central Italy. *Journal of Volcanology and Geothermal Research*, *177*(2), 500–514. https://doi.org/10.1016/j.jvolgeores.2008.07.016

Rovere, A., Raymo, M. E., Vacchi, M., Lorscheid, T., Stocchi, P., Gomez-Puol, L., et al. (2016). The analysis of Last Interglacial (MIS 5e) relative sea-level indicators: Reconstructing sea-level in a warmer world. *Earth-Science Reviews*, *159*, 404–427. https://doi.org/10.1016/j.earscirev.2016.06.006

Sevink, J., di Vito, M. A., Piochi, M., Mormone, A., van Gorp, W., & Bakels, C. C. (2018). A rare Mid-Würmian lithoid tuff in the Agro Pontino graben (Southern Lazio, Italy) and its identification as an Albano 5–7 related distal tephra deposit (41–36 kaBP): Characteristics, provenance and paleogeographical implications. *Annals of Geophysics*, *61*(1), S109. https://doi.org/10.4401/ag-7574

Sevink, J., Vos, P., Westerhoff, W. E., Stierman, A., & Kamermans, H. (1982). A sequence of marine terraces near Latina (Agro Pontino, central Italy). *Catena*, *9*(1–2), 361–378. https://doi.org/10.1016/s0341-8162(82)80023-4

Stiner, M., & Kuhn, S. (1992). Subsistence, technology and adaptive variation in the middle paleolithic. *American Anthropologist*, *94*(2), 306–339. https://doi.org/10.1525/aa.1992.94.2.02a00030

Stocchi, P., Vacchi, M., Lorscheid, T., de Boer, B., Simms, A. R., van de Wal, R. S. W., et al. (2018). MIS 5e relative sea-level changes in the Mediterranean Sea: Contribution of isostatic disequilibrium. *Quaternary Science Reviews*, *185*, 122–134. https://doi.org/10.1016/j.quascirev.2018.01.004

Taschini, M. (1979). L'industrie lithique de Grotta Guattari au M. Circé, Latium: Définition culturelle, typologique et chronologique du Pontinien. *Quaternaria*, *21*, 179–247.

Vicens, D., Gràcia, F., & Ginés, A. (2012). Quaternary beach deposits in Mallorca: Paleontological and geomorphological data. In A. Ginés, J. Ginés, L. Gómez-Pujol, B. P. Onac, & J. J. Fornós (Eds.), *A Mediterranean benchmark for Quaternary studies. Monografies de la Societat d'Història Natural de les Balears. Mallorca* (Vol. 18, pp. 55–83). Retrieved from http://www.shnb.org/monografies/monografia18/Mon_Soc_Hist_Nat_Balears_18_2012.pdf

Villa, P., Soriano, S., Pollarolo, L., Smriglio, C., Gaeta, M., D'Orazio, M., et al. (2020). Neandertals on the beach: Use of marine resources at Grotta dei Moscerini (Latium, Italy). *PLoS One*, *15*(1), e0226690. https://doi.org/10.1371/journal.pone.0226690

Wehmiller, J. F., Simmons, K. R., Cheng, H., Lawrence Edwards, R., Martin-McNaughton, J., York, L. L., et al. (2004). Uranium-series coral ages from the US Atlantic Coastal Plain—The "80 ka problem" revisited. *Quaternary International*, *120*(1), 3–14. https://doi.org/10.1016/j.quaint.2004.01.002

Wulf, S., Keller, J., Paterne, M., Mingram, J., Lauterbach, S., Opitz, S., et al. (2012). The 100–133 ka record of Italian explosive volcanism and revised tephrochronology of Lago Grande di Monticchio. *Quaternary Science Reviews*, *58*, 104–123. https://doi.org/10.1016/j.quascirev.2012.10.020

Zei, M. (1979). Una spiaggia tirreniana a Strombus su un fondale marino a Est del M. Circeo. *Studi per l'Ecologia del Quaternario*, *1*, 13–17.

References From the Supporting Information

Schwarcz, H. P., Buhay, W., Grün, R., Stiner, M., Kuhn, S., & Miller, G. H. (1990–91). Absolute dating of sites in coastal Lazio. *Quaternaria Nova*, *1*, 51–67.